Prediction of the thermal degradation–induced colour change of acrylonitrile butadiene styrene products as a function of temperature and titanium dioxide content

Virág Á. D., Suplicz A., Török D.

Results in Engineering 24 (2024) 103505

Contents lists available at ScienceDirect

Results in Engineering

journal homepage: www.sciencedirect.com/journal/results-in-engineering

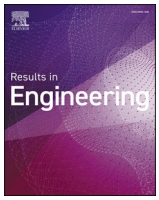

Research paper

Prediction of the thermal degradation–induced colour change of acrylonitrile butadiene styrene products as a function of temperature and titanium dioxide content

Ábris Dávid Virág [a], András Suplicz [a,b,*], Dániel Török [a,b]

[a] Department of Polymer Engineering, Faculty of Mechanical Engineering, Budapest University of Technology and Economics, Műegyetem rkp. 3., H-1111 Budapest, Hungary
[b] MTA-BME Lendület Lightweight Polymer Composites Research Group, Műegyetem rkp. 3., H-1111 Budapest, Hungary

ARTICLE INFO

Keywords:
Colour prediction
CIELAB
Colouring agent
Master curve
ABS
TiO_2

ABSTRACT

In this study, we examined the thermal degradation–induced colour change of acrylonitrile butadiene styrene (ABS)–based titanium dioxide (TiO_2)–doped products as a function of TiO_2 content and temperature. Based on the time–temperature superposition (tTS) principle and the CIELAB colour space, we proposed a methodology for developing a robust model to estimate the long-term colour change of polymers doped with TiO_2 at elevated temperatures. We used 800 h of measurement data to develop the model and validated the colour change predictions of the model in 1600 h. The average colour difference between the measured and modelled results at the application temperature range (below 80 °C) was <1.5, smaller than the just noticeable difference (*JND*) in the CIELAB colour space. We found that above a certain TiO_2 content (approximately 3 wt%), the colour retention of the ABS/TiO_2 specimens can no longer be improved by increasing their TiO_2 content. To show the applicability of the model, we present two simple case studies predicting the colour and appearance of a polymer product under constant and variable heat loads. The proposed methodology provides an excellent tool for design, as it can be used to determine the optimum amount of TiO_2. Moreover, it accelerates and simplifies the design process.

1. Introduction

A product's colour is a key design element in many industrial applications. From a marketing perspective, colour strongly shapes the consumer's view of a product as it can affect the purchase intention [1] by influencing the perception of several properties, such as healthfulness [2], flavour [3], or size/portion [4]. From an engineering point of view, colour change is crucial, as several processes/treatments and environmental effects can result in a change of colour, e.g. radiation [5] and heat [6] treatments or fermentation processes [7]. For this reason, colour (specifically colour change) is often used as an indicator. There is a wide range of applications for process monitoring and product rating based on colour change, from the quality control of heat-treated wood products [8] through the condition monitoring of synthetic hydraulic oils [9] to high-performance colourimetric humidity sensors [10–13].

The primary colour of a polymer product can be modified by fillers/reinforcing materials [14] and colouring agents such as dyes or colourants [15,16]. However, due to different environmental influences, polymer products may change colour. This colour change (most often yellowing in the case of polymers) can severely limit a product's acceptance by users or even functional use in areas where transparency and clear white colour are required.

Yellowing has two main causes. The first reason may be the degradation of the polymer itself, especially in the case of polyaromatics (e.g. polyesters, epoxy amines or polystyrene). The degradation of the polymer can occur during melt processing or end-use [17]. Secondly, the discolouration can be caused by the by-products of additives. The structural stability of thermal antioxidants used for stabilisation influences the rate of yellowing [18]. Pastorelli et al. [19] investigated the effects of different environmental parameters on polymer degradation and discolouration. Their study on 17 different polymers showed that light and nitrogen dioxide concentration are the dominant factors for colour change. Wu et al. [20] studied the thermal and ultra-violet (UV) light–induced yellowing of epoxy and vinyl ester resins. Thermal ageing produced a darker colour (higher yellowness index) with the same exposure time. They found that a radical oxidation reaction causes the

* Correspondig author.
E-mail address: suplicz@pt.bme.hu (A. Suplicz).

https://doi.org/10.1016/j.rineng.2024.103505
Received 10 June 2024; Received in revised form 29 October 2024; Accepted 22 November 2024
Available online 3 December 2024

yellowing of the resins, and it can be prevented or reduced with coatings, antioxidants, and UV absorbers.

The extent of yellowing can be estimated with appropriate models if the environmental effect causing it is known. Achtioui et al. [21] presented a model to predict the yellowing of styrene-stat-acrylonitrile (SAN) and acrylonitrile-butadiene-styrene (ABS) during processing with an internal mixer. The effects of temperature, rotation speed and residence time were considered, and a good correlation was found between yellowing and mixing energy. Matsuo et al. [22] conducted accelerated ageing treatment on hinoki wood and analysed the colour changes. The time–temperature superposition (tTS) principle was applied to describe the temperature dependence of the reaction rate. Then, they used kinetic analysis to predict the time–dependent changes of the CIELAB colour coordinates (L^*, a^*, b^*) caused by thermal oxidation during natural ageing. Mochizuki and Takayama [23] also applied tTS to predict colour changes in liquid formulations. The authors applied accelerated ageing treatment at elevated temperatures and measured the CIELAB colour coordinates. The tTS principle gave reliable predictions for colour change over time. Wu et al. [24] constructed back propagation artificial neural networks (BP-ANNs) to predict the degradation of polycarbonate (PC) in different environments. Significant environmental parameters were determined, and the results were verified with weathering tests in new locations. The authors presented a predictive map for PC degradation based on the yellowness index (YI). Liu et al. [25] investigated the effects of UV light on photovoltaic modules (solar panels). The authors quantified colour change with the YI and found a linear relationship between the YI and UV irradiation dose.

Additives are often used to overcome discolouration in polymer products. Titanium dioxide (TiO_2) has been widely studied for its photocatalytic effects and is commonly used as a colouring (whitening) agent for polymers [26–28]. R.E. Day [29] investigated the effects of TiO_2 pigments on thermoplastic polymers. They showed that due to its good UV absorbing capability, TiO_2 can prevent photoaging and mask the yellowing effect. Semperger et al. [30] also demonstrated the positive effects of TiO_2 as a UV stabiliser in the case of PA6. Asiaban et al. [31] found that TiO_2 pigments can reduce the intrinsic yellowness of ABS. However, the pigment can decrease impact strength and hardness when applied in higher amounts (above 1.5 wt%). Han et al. [32] showed that TiO_2 can promote hydrophilicity when added to ABS. Therefore, TiO_2-ABS composites have the potential to be membranes for oil/water separation.

While TiO_2 is extensively used as an additive in the plastics industry, no established models exist to predict the heat-induced colour change in TiO_2-doped plastic products, marking a knowledge gap in the literature. This study addresses this gap by introducing a novel modelling approach to predict the colour change in ABS products over time based on temperature and TiO_2 concentration. For this purpose, ABS/TiO_2 injection-moulded plates with six different TiO_2 concentrations were produced, subjected to thermal ageing at five distinct temperatures, and monitored for colour change using CIELAB measurements over an 800-hour period. This comprehensive dataset enabled the development of a predictive model, followed by two case studies demonstrating its practical application in a simulation environment. The model's development and validation through 1600 h of CIELAB colour measurements under controlled thermal ageing provides a robust foundation for its use in simulation environments. This application enables manufacturers to forecast product appearance changes before production, supporting quality control and material optimisation for long-term aesthetics and stability.

2. Materials and methods

2.1. Materials

The acrylonitrile butadiene styrene (ABS) used in this study was an injection moulding grade

ABS, namely Terluran GP 35 (supplied by INEOS Styrolution, Frankfurt am Main, Germany), with a density of 1.04 g/cm^3 and a melt volume rate (220 °C/10 kg) of 34 cm^3/10 min according to the manufacturer's data. As a whitening agent, we used rutile-type titanium dioxide (TiO_2) KTR600 supplied by Ixom Operations Pty Ltd. (Auckland, New Zealand), which has the following CIELAB colour values (according to the manufacturer's data): L^*=97.78, a^*=−0.34, b^*=2.62.

2.2. Compounding

The ABS-based compounds were prepared with an LTE 26–44 twin-screw extruder (Labtech Engineering Co., Ltd., Thailand) with a length/diameter ratio (L/D) of 44 and a screw diameter of 26 mm. Before processing, the ABS was dried in a Faithful WGLL-125 BE (Faithful Instrument (Hebei) Co., Ltd., Huanghua, China) hot air oven at 80 °C for 4 h. Before extrusion, the TiO_2 was added to the ABS by dry mixing at different percentages by weight: 0, 0.2, 0.5, 0.7, 1, 2.5, 5, 7.5 and 10 wt %. The temperature profile from hopper to die was: 200–200–205–205–210–210–215–215–220–220 °C. The die temperature was 220 °C, and the screw speed was 60 rpm. The extrudate was pelletised using an LZ-120/VS (Labtech Engineering, Thailand) granulator, and these pellets were used for injection moulding.

2.3. Injection moulding

Injection moulding was carried out using a two-cavity, cold runner mould with an Arburg Allrounder Advance 270S 400–170 (ARBURG GmbH, Germany, Lossburg) injection moulding machine. We produced 80 × 80 mm, 2 mm thick plate specimens from the compounded pellets. The temperature profile from hopper to nozzle was 225, 230, 235, 240 and 240 °C, while the mould temperature was 30 °C. The screw ($D = 30$ mm, $L/D = 20$) had a screw speed of 25 rpm, and shot volume was 45 cm^3. The injection rate was 45 cm^3/s, and the switchover was set to 8.5 cm^3. Peak injection pressure reached 702 bar, and holding pressure was maintained at 500 bar for 5 s. The residual cooling time was 15 s. The total cycle time was 27.1 s.

2.4. Thermal ageing

The thermal ageing of the injection-moulded plate specimen containing 0, 1, 2.5, 5, 7.5 and 10 wt% TiO_2 was carried out in a Faithful WGLL-125 BE hot-air oven (Faithful Instrument (Hebei) Co., Ltd., Huanghua, China), a Faithful DZ-3BCII hot-air oven (Faithful Instrument (Hebei) Co., Ltd., Huanghua, China) and a Venticell LSIS-B2V/VC55 hot-air oven (MMM Medcenter Einrichtungen GmbH, Planegg, Germany) at the following temperatures: 60, 70, 80, 90 and 100 °C. In all cases, the heat exposure time was 800 h (~33 days). However, to validate our predictions to a certain extent, we continued the test at 80 °C until 1600 h (~67 days).

2.5. Measurement of CIELAB colour values

To characterise the colour change of the tested samples, we used the CIELAB three-dimensional colour space with L^*, a^* and b^* colour values. L^* refers to the achromatic colour (lightness or greyness) from 0 (black) to 100 (white). a^* and b^* represent redness (-a^*) /greenness (+a^*) and blueness (-b^*)/yellowness (+b^*), both indicating chromatic ("real") colour. Therefore, in this colour space, each colour is represented by a point with L^*, a^* and b^* coordinates in the CIELAB colour space. The colour values were measured with a Gardner BYK colour guide sphere spectrophotometer (BYK-Gardner GmbH, Geretsried, Germany) under a D65 CIE standard illuminant light source at an observer angle of 10° Colour measurements were taken on 3 different samples at 3 points per sample in every case, resulting in nine data points per material and treatment temperature. The maximum standard deviation of the nine

measurement points was 3.3, 0.9 and 1.6 for the L^*, a^* and b^*, respectively. Based on the resulting standard deviations, the total colour difference (ΔE^*_{ab}), which is an industry-wide significant characteristic, can be considered. ΔE^*_{ab} is the linear distance in CIELAB colour space between the two sets of coordinates ($\Delta E^*_{ab} = \sqrt{\Delta L^{*2} + \Delta a^{*2} + \Delta b^{*2}}$). For the measured L^* colour coordinates having the highest standard deviation, if a^* and b^* were the same, this difference would result in a ΔE^*_{ab}=3.3. Depending on the field of industrial use, this value can be acceptable. Considering these, we used the average colour values in the calculations.

We measured the L^*, a^* and b^* colour values of the samples, throughout the thermal ageing period, carrying out one measurement per weekday. Colour measurements on the specimen containing 0.2, 0.5, 0.7 wt% TiO_2 were performed only at ageing time $t = 0$ s.

2.6. Generating the master curve and modelling

Data analysis, model development and fitting were performed in Matlab R2021a software (Mathworks, Natick, MA, USA). We used the coefficient of determination (R^2) and the root mean squared error (*RMSE*) to rate the goodness of fitting to the models.

3. Results and discussion

3.1. Development of a model to predict colour change

To predict the thermal degradation–induced colour change of ABS-based TiO_2-doped products as a function of TiO_2 content (w) and temperature (T) at any arbitrary $t > 0$ time point, we developed a robust model. The steps of developing the model are summarised in Fig. 1.

3.1.1. Generating the master curve and determining the shift factor (temperature dependence)

As the first step, we applied the time-temperature superposition (tTS) principle (described in detail by Ferry [33]) to predict colour changes from a few hundred hours of measurements over a period of years. Using tTS, we constructed a master curve from the mean colour data (L^*, a^*, b^*) measured at different temperatures for each w. The arbitrary colour value is hereafter denoted by X. The datasets measured at different temperatures were shifted along the time axis to coincide with the data obtained at the reference temperature, $T_{ref} = 80$ °C, until a continuous curve was obtained. This procedure results in the concept of reduced time (t_{red}), which is defined by Eq.1. Thus, data measured at temperatures other than T_{ref} can be "reduced" to T_{ref} with the use of Eq.1, resulting in the extension of the initial measurement time range (Fig. 2/a).

$$t_{red}|_{T=T_{ref},\ w=const.} = \frac{t|_{T=const.,\ w=const.}}{a_{T\_X}(T)|_{w=const.}} \tag{1}$$

where a_{T_X} is the time shift factor for the X colour value at a given w.

We performed this procedure for all three colour values, and then fitted an exponential model (Eq.2) to the generated master curves (Fig. 2/b):

$$X(t_{red})|_{T=T_{ref}} = k_{1\_X} + k_{2\_X} \cdot e^{k_{3\_X}\log(t_{red})} \tag{2}$$

where k_{1_X} was calculated as the mean of the first 150 points and k_{2_X}, k_{3_X} are fitted constants. k_{1_X} indicates the initial colour value ($k_{1\_X} = X|_{t=0}$), and k_{2_X} and k_{3_X} determine the colour change rate. The master curves were generated with the mean values, but fitting was performed with the use of all the measured data.

In the second step, we investigated the temperature dependence of

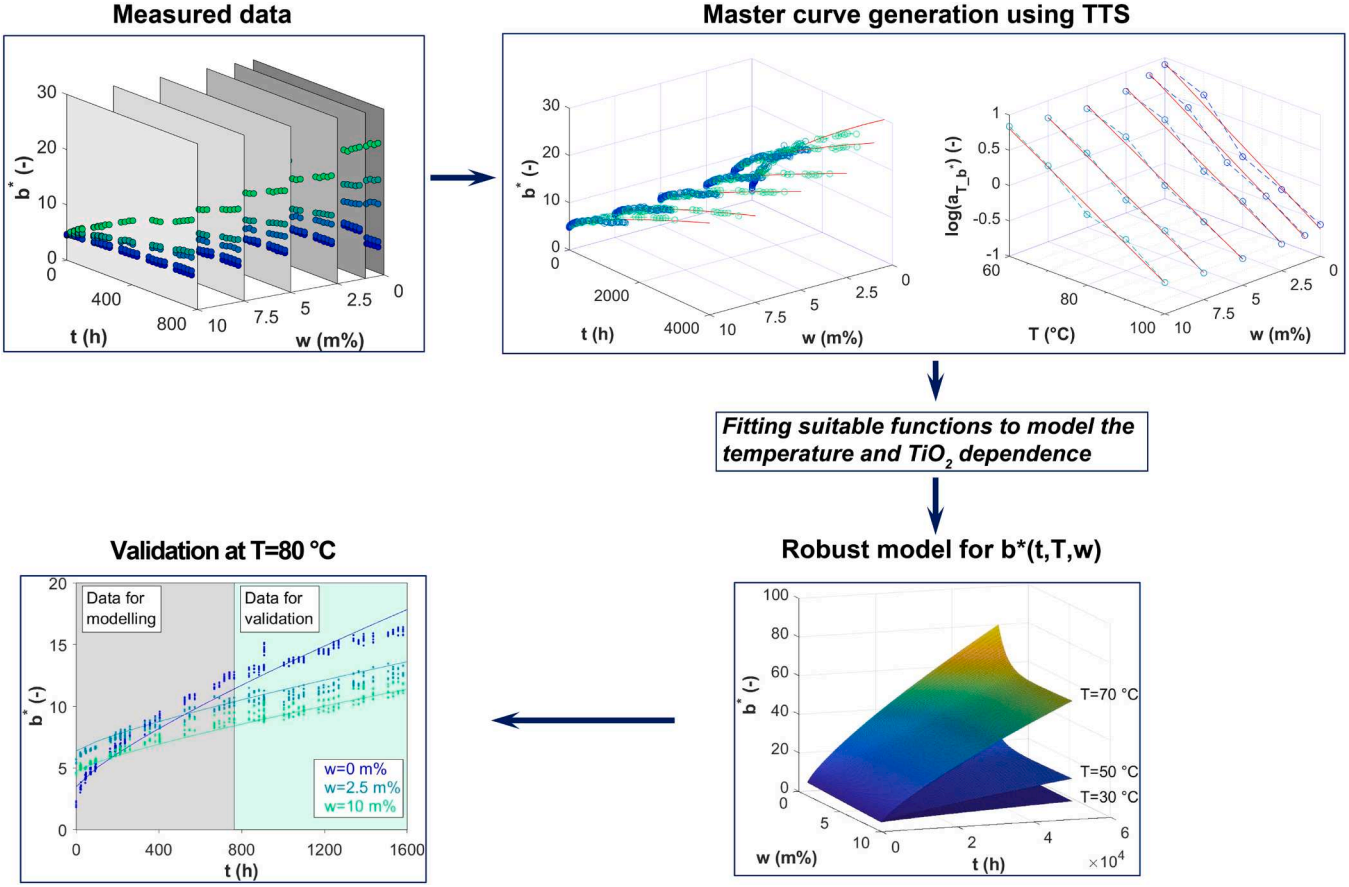

Fig. 1. Steps of developing the model to predict colour change as a function of temperature and titanium dioxide content presented for the b^* colour component.

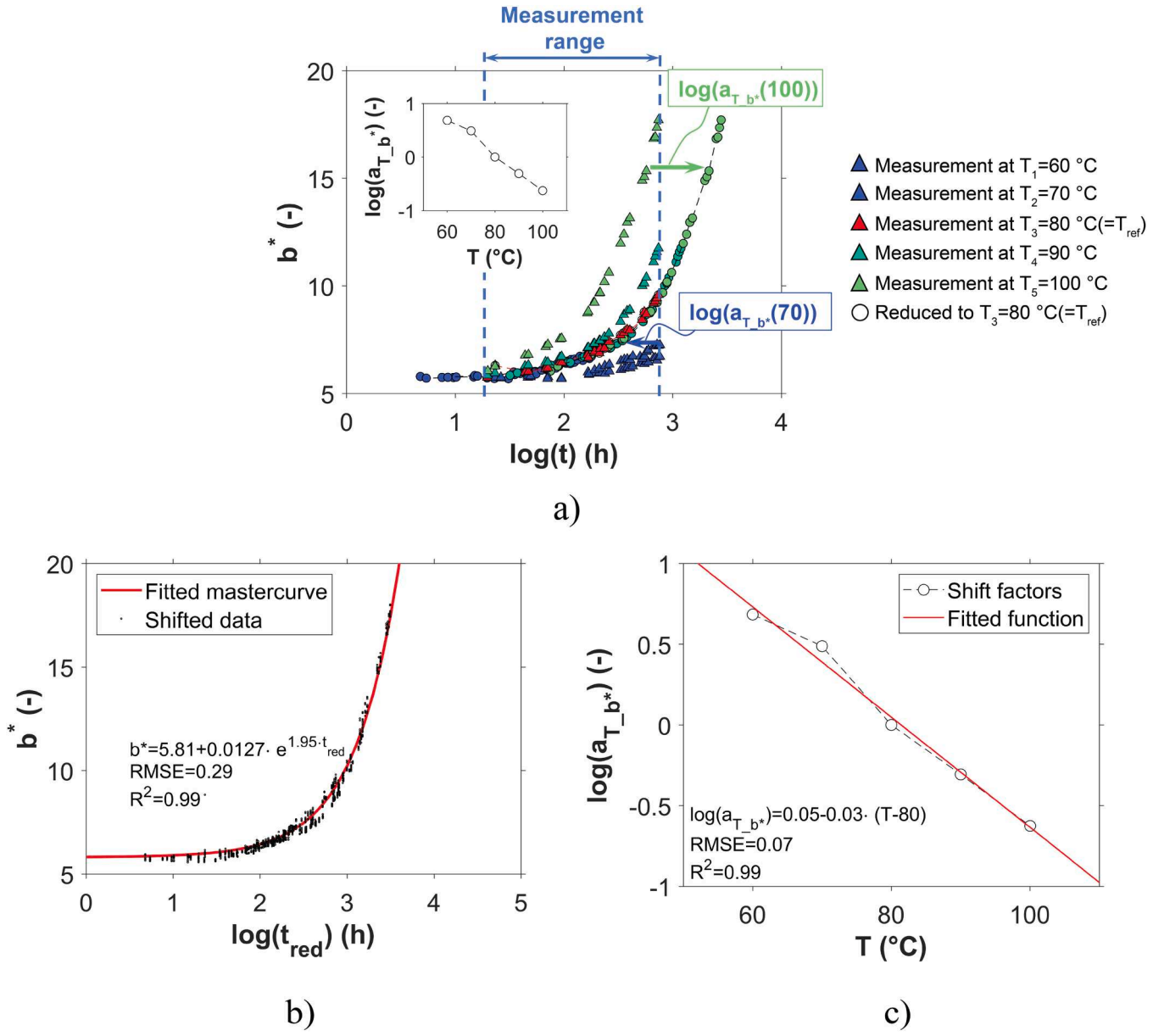

Fig. 2. Mean values of measured data (for $w = 5$ wt%) and the generated master curve at $T_{ref} = 80$ °C for the b^* colour component (a), exponential model fitted to the master curve with the use of all the measured data (b), fitted linear function to describe the temperature dependence of the shift factor (c).

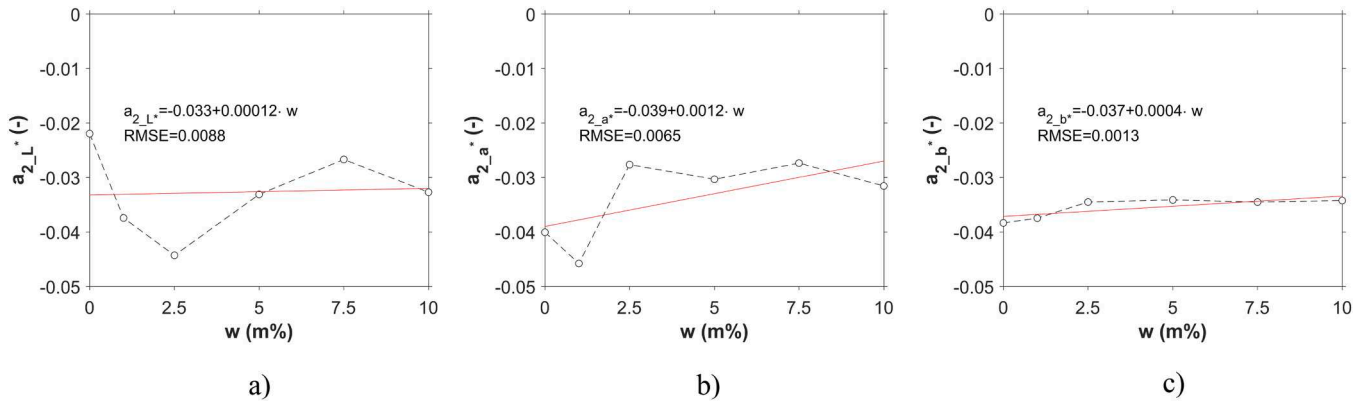

Fig. 3. Titanium dioxide content-dependence of the slope of the linear trend (a_{2_x}), which describes the temperature dependence of the shift factors for the L^* (a), a^* (b) and b^* (c) colour values.

the resulting a_{T_X} for each w. We found that $a_{T\_X}(T)$ can be well described by Eq.3 for every w (Fig. 2/c):

$$\log\left(a_{T\_X}(T)|_{w=const.}\right) = a_{1\_X} + a_{2\_X}\cdot\left(T - T_{ref}\right) \quad (3)$$

where a_{1_X} and a_{2_X} are fitted constants. a_{1_X} was included because the temperature may have fluctuated. Therefore, it was used for the fitting, but later on, we did not use it; only a_{2_X} was used for the model. As a result of the first two steps, we can predict the colour change of ABS-based TiO_2-doped samples at different temperatures over a long period of time at a fixed w. To predict this colour change for any desired w, we need two further steps.

3.1.2. *Investigating the effects of titanium dioxide content (titanium dioxide dependence)*

In the third step, we investigated the TiO_2-dependence of the slope of the linear trend (a_{2_X}), which describes the temperature dependence of the shift factors for all three colour values (Fig. 3). Based on previous results [34,35], we assumed that increasing TiO_2 content would reduce the effect of temperature on the samples' colour change. This means the absolute value of a_{2_X} parameters will decrease with increasing TiO_2 content. We assumed an increasing trend in the $a_{2\_a^*}$ and $a_{2\_b^*}$ parameters with increasing TiO_2 content. These results indicate that an increase in TiO_2 content reduces the change of the a^* and b^* colour values due to temperature. The results for $a_{2\_L^*}$ did not show a trendwise change. However, based on the work of Bersch et al. [36] whose results showed a linear trend in the change of L^* due to the increase in TiO_2 content, we approximated all of these dependencies with linear functions (Eq. (4)):

$$a_{2\_X}(w) = a_{21\_X} + a_{22\_X}\cdot w \quad (4)$$

where $a_{11\_L^*}$, $a_{12\_L^*}$, $a_{11\_a^*}$, $a_{12\_a^*}$, $a_{11\_b^*}$, $a_{12\_b^*}$ are fitted constants. Based on Eqs.3 and 4, the T and TiO_2 content-dependent shift factor ($a_{T\_X}(T,w)$) can be determined.

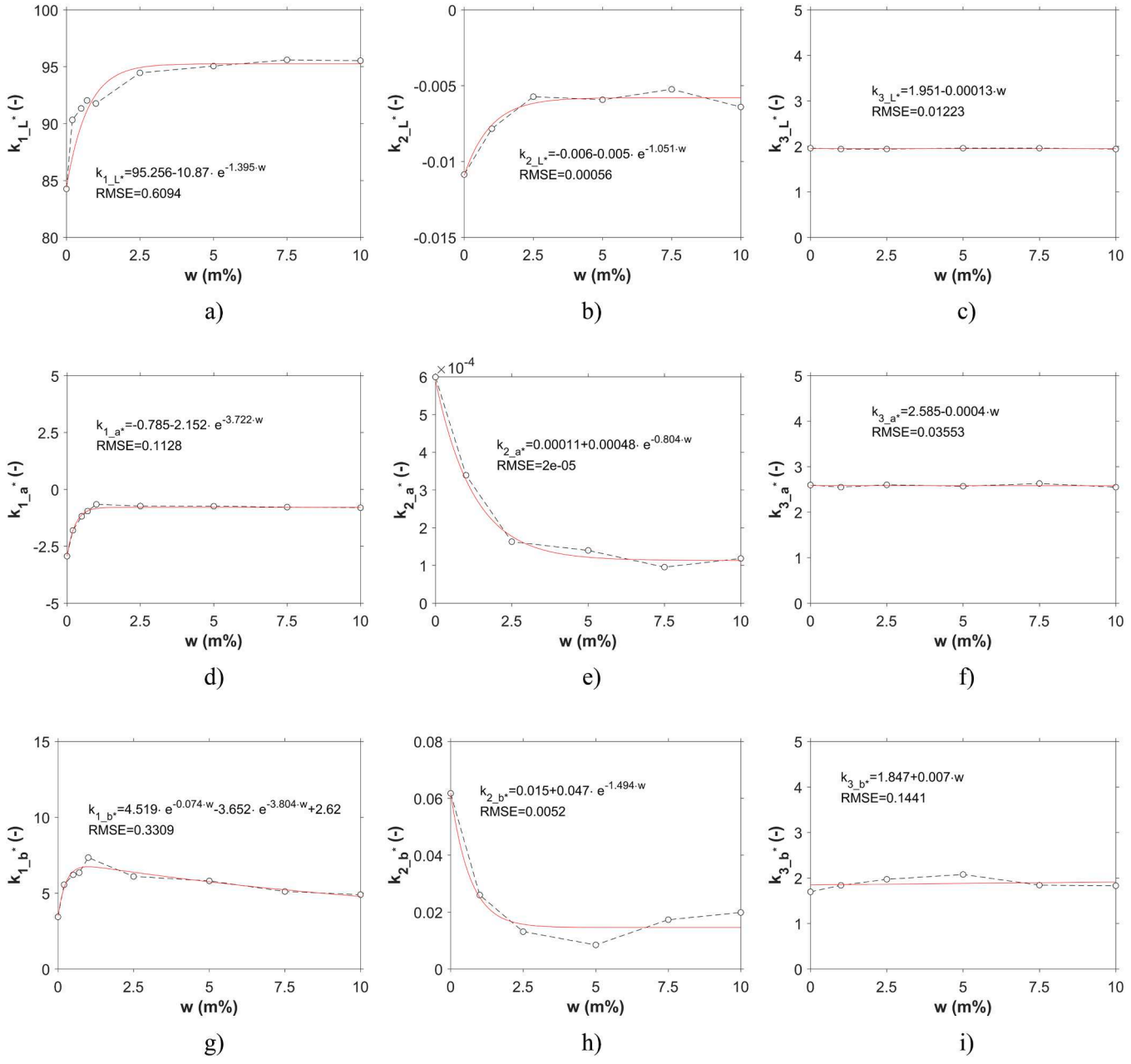

Fig. 4. Titanium dioxide content-dependence of the parameters of master curves describing the time-dependent change of colour values. The circles denote the exact values, continuous lines are the fitted suitable functions for L^*(a-c), a^*(d-f) and b^* (g-i) colour values.

In the fourth step, we examined the dependence of the master curve model parameters of Eq.2 on TiO_2 content (Fig. 4). These dependencies were approximated using suitable saturation and decay exponential and linear functions (Eq.5–9).

$$k_{1\_L^*}(w) = k_{11\_L^*} + k_{12\_L^*} \cdot e^{k_{13\_L^*} \cdot w} \tag{5}$$

$$k_{1\_a^*}(w) = k_{11\_a^*} + k_{12\_a^*} \cdot e^{k_{13\_a^*} \cdot w} \tag{6}$$

$$k_{1\_b^*}(w) = k_{11\_b^*} \cdot e^{k_{12\_b^*} \cdot w} + k_{13\_b^*} \cdot e^{k_{14\_b^*} \cdot w} + k_{15\_b^*} \tag{7}$$

$$k_{2\_X}(w) = k_{21\_X} + k_{22\_X} \cdot e^{k_{23\_X} \cdot w} \tag{8}$$

$$k_{3\_X}(w) = k_{31\_X} + k_{32\_X} \cdot w \tag{9}$$

where $k_{1\_L^*}$, $k_{1\_a^*}$ and $k_{1\_b^*}$ are the initial L^*, a^* and b^* colour values, respectively. k_{2_X} and k_{3_X} are the parameters characterising the degree of change in the given colour component. The parameters containing two numbers in the subscript are fitted values. For the $k_{1\_L^*}$, $k_{1\_a^*}$ and $k_{1\_b^*}$ values to be correct, these values must be the L^*, a^* and b^* colour values of TiO_2 at $w = 100$, respectively. Therefore, the colour component data of TiO_2 were used to fit the models.

Between 0 and 1 wt% TiO_2 content, we observed an abrupt change in the k_{1_X} values (Fig. 4/a,d,g). We also determined the initial colour values for samples containing 0.2, 0.5 and 0.7 wt% TiO_2 to find suitable functions. With increasing TiO_2 content, the $k_{1\_L^*}$ and $k_{1\_a^*}$ parameters reach saturation at a certain level, while $k_{1\_b^*}$ increases to 1 wt% and steadily decreases thereafter (Fig. 4/a,d). This suggests that with increasing TiO_2 content, the colour of the ABS sheets becomes lighter and slightly redder. In addition, up to 1 wt%, the colour tends to shift towards yellow and then increasingly towards blue. However, regarding the L^* and a^* colour values, these curves become saturated, i.e. increasing the TiO_2 content above approximately 3 wt% does not lead to further changes in these colour values. At this amount, the values of L^* and a^* of the applied TiO_2 additive are already reached. The rate of change of the colour component due to heat can be reduced by TiO_2 doping above a certain TiO_2 content, but the temperature resistance of the specimen does not increase further.

After the decrease in absolute value, the k_{2_X} parameters all saturate with increasing TiO_2 content (Fig. 4/b,e,h). This means that the rate of change of the colour component due to heat can be reduced by TiO_2 doping. But above a certain TiO_2 content (approximately 3 wt%), the colour retention of the ABS specimens is no longer improved. With increasing TiO_2 doping, the sample becomes less dark (increasing $|L^*|$ values) and less shifted towards yellow (decreasing b^* values) or red (decreasing a^* values) due to thermal load. k_{3_X} was found to be quasi-constant in all three cases (Fig. 4/c,f,i). Therefore, after fixing the values of k_{3_X}, we performed the fitting of Eqs. (5)-(9) again and used the resulting fitting parameters for the model.

3.1.3. Generating and validating the models

Based on the four steps described in Section 3.1.1 and 3.1.2, robust models can be defined, which express the colour values as a function of t, T and TiO_2 content (Eq.10):

$$X(t,\ T, w) = k_{1\_X}(w) + k_{2\_X}(w) \cdot e^{k_{3\_X} \cdot \log\left(\frac{t}{a_{T\_X}(T,w)}\right)} \tag{10}$$

where k_{1_X} and k_{2_X} are the initial value and the rate of the change in colour component value, respectively (both are TiO_2 content–dependent parameters), while k_{3_X} is independent of TiO_2 content, it only depends on the colour component. The model resulting from Sections 3.1.1 and 3.1.2 can predict the colour of ABS-based TiO_2-doped products as a function of TiO_2 content (w) and temperature (T) at an arbitrary time $t > 0$. Fig. 5 shows the time-dependent and TiO_2 content–dependent surfaces generated from the model at different temperatures for each colour component.

We rated the goodness of fit for the model with several metrics. The root mean squared error (*RMSE*) values (Fig. 6/a-c) were <2.5 in all the cases tested, except for the b^* colour component of the $w = 0$ wt% sample at $T = 100$ °C, where the error was 8.4. Note, that the glass transition temperature (T_g) of ABS is around 105 °C [37] and near the T_g mechanical problems can already arise. Although it was important to carry out colour measurements at temperatures close to T_g for long-term tTS-based predictions, the real application temperature of ABS is below 80 °C. In the cases of real application temperatures the *RMSE* values for the b^* colour component were <1.4 in all cases. Moreover, the *RMSE* values for a^* and L^* were significantly lower. These results suggest that all three colour values can be well estimated using the developed model. The largest deviation from the actual values obtained in the greenness/yellowness component, and there are actually marginal errors for the green/blue component and for the lightness. We also examined how the squared errors evolved with the samples measured at 80 °C, where we had data beyond the data used for modelling (data from 0 to 800 h). Based on Fig. 6/d-f, we found that the squared errors between 800 and 1600 h are even smaller, meaning that in this region our model gives an even more accurate prediction for each colour component. To rate the colour difference between the measured and the modelled results we calculated the average colour difference (ΔE_{avg}) from Eq. (11):

$$\Delta E_{avg} = \sqrt{\frac{1}{n}\sum_{i=1}^{n}\left(L_{model,i} - L_{measured,i}\right)^2 + \left(a_{model,i} - a_{measured,i}\right)^2 + \left(b_{model,i} - b_{measured,i}\right)^2} \tag{11}$$

where n is the number of measured data for the given (t,w) pairs.

Fig. 6/g shows that ΔE_{avg} is <2.8 in all cases, but the $w = 0$ % case at $T = 100$ °C (where it is 7.0). Moreover, if we consider the actual application temperature range, i.e. below 80 °C, ΔE_{avg} is <1.5 in all cases. In the CIELAB colour space, $\Delta E_{avg} = 2.3$ corresponds to the just noticeable difference (*JND*) value [38], which means that *JND* is the amount that a given colour has to be modified to obtain a noticeable difference. Therefore, within the actual application temperature range, the model can provide an accurate estimate with a colour difference smaller than *JND*.

Consequently, the proposed methodology can be used to estimate the long-term colour change of polymers doped with TiO_2 at elevated temperatures, as a function of the amount of TiO_2 added. Therefore, it is an excellent tool for design, as it can be used to estimate the appearance of a product exposed to elevated temperatures.

3.2. Practical application: case studies

3.2.1. The prediction of colour for a constant heat load

One possible application of the model is to determine the colour change of a polymer product under constant heat load. If we know the conditions under which our polymer product will be used (e.g. at what temperature and for how long it will be exposed to heat), we can use the model to estimate the colour change, even over years. Fig. 7/a shows the measurement points used for model fitting and the solid line provided by the model. Green dots indicate the four different time points at which

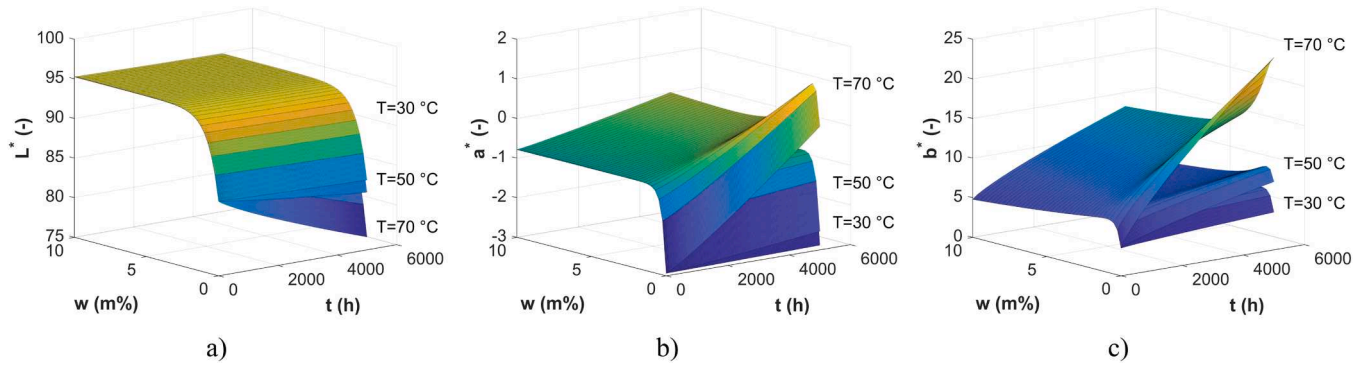

Fig. 5. The generated model represented as a surface for each colour component at different temperatures showing how the model depends on time and titanium dioxide content for L^* (a), a^* (b) and b^* (c) colour values.

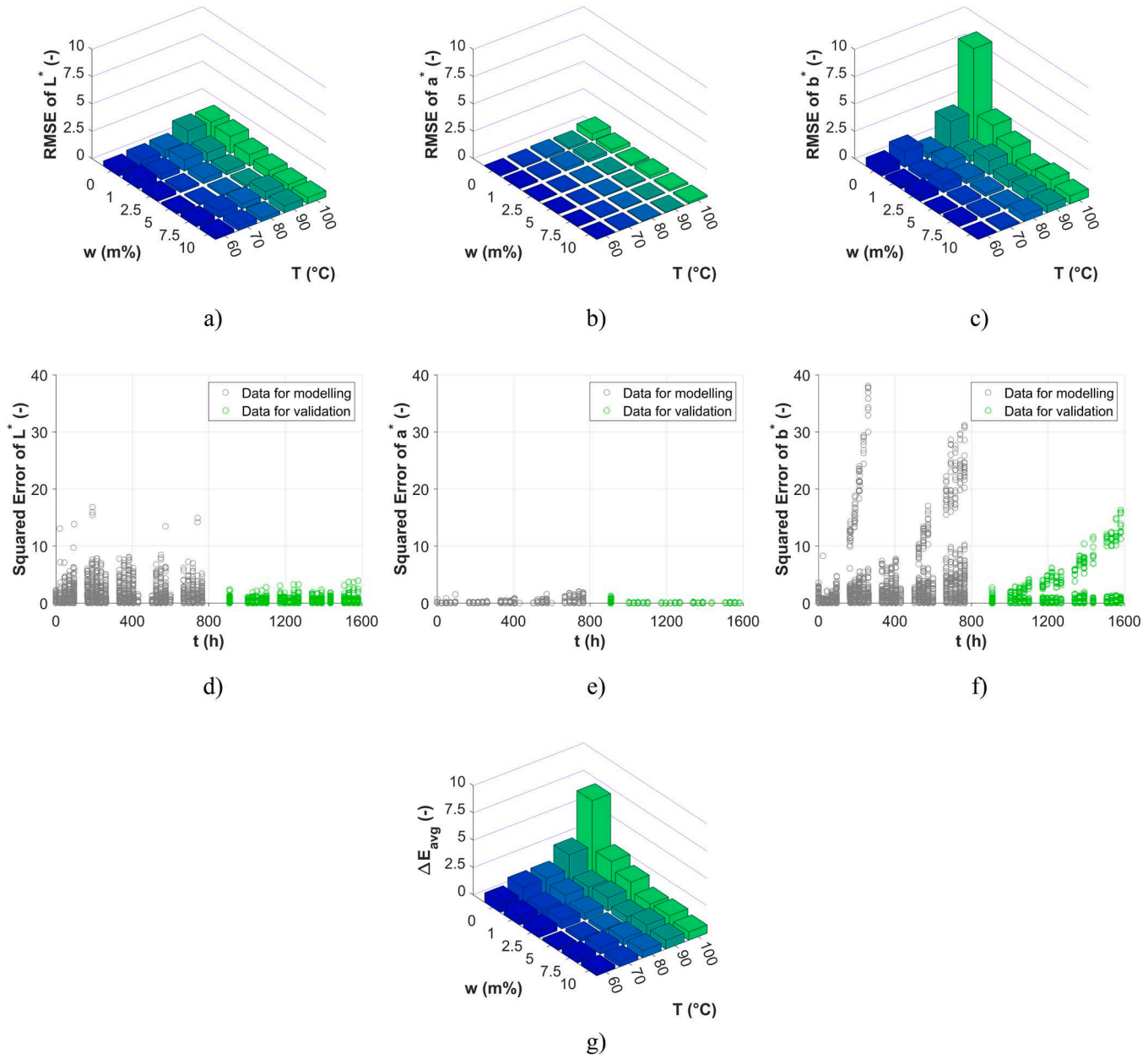

Fig. 6. Root mean squared errors (RMSE) of the model for the data used for modelling for L^* (a), a^* (b) and b^* (c) colour values the squared errors for modelling and validation for L^* (d), a^* (e) and b^* (f) colour values, and the average colour difference (ΔE_{avg}) for every examined case (g).

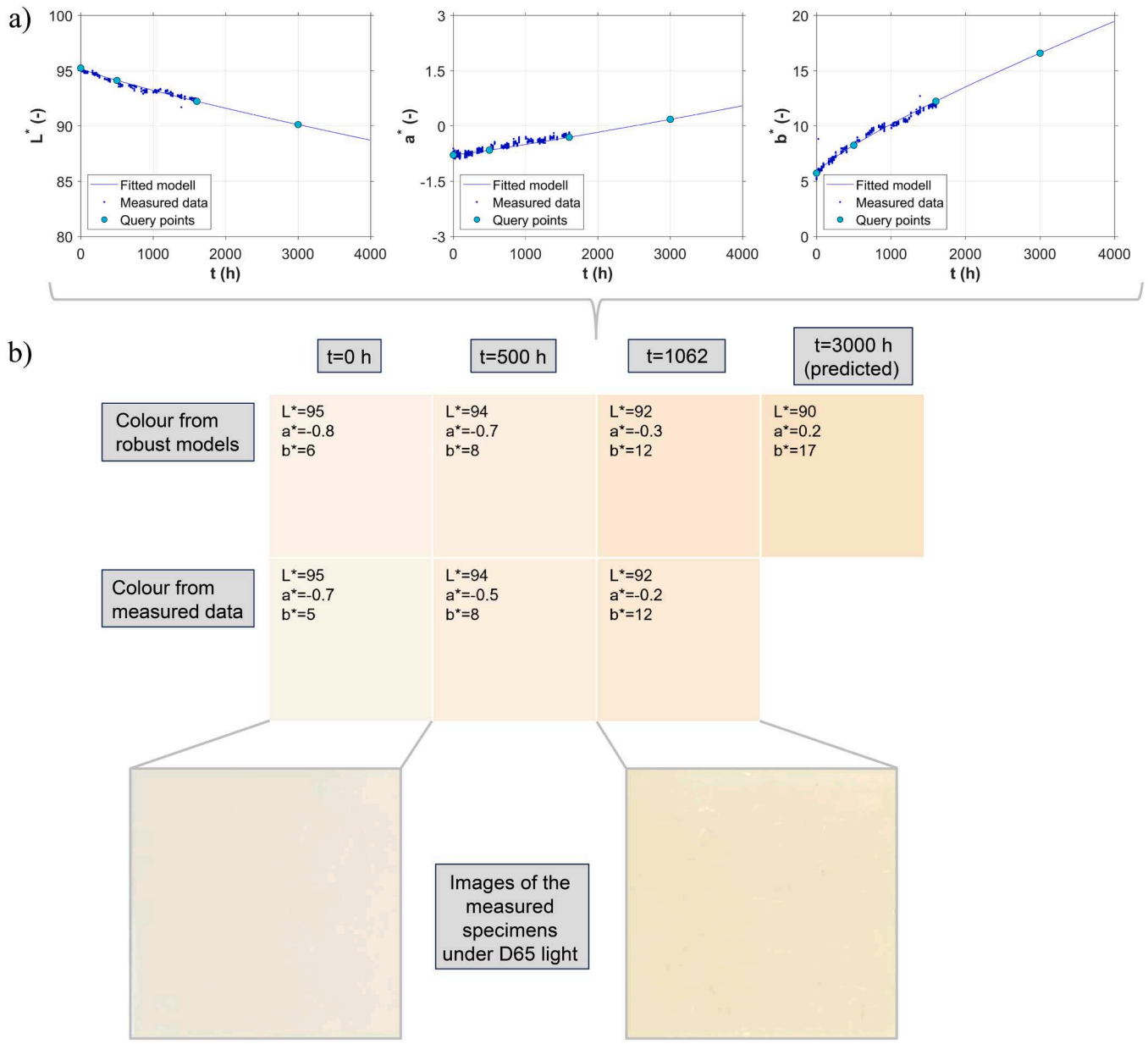

Fig. 7. Comparison of the predicted colour and the measured colour of the sample exposed to constant heat load for the $w = 5$ wt% case at $T = 80$ °C.

the estimated colour of the test specimen was obtained based on the model. The first three are the measured points, where the first two were used for model fitting and the third for validation. The fourth point shows the predicted colour change based on the model. Then, we compared the predicted colour values with the actual data. Based on the obtained colour values, we displayed the colour of the test specimens (Fig. 7/b). At the points where measured data were available, the discrepancy between the data estimated by the model and the measured data is negligible. Also, the plate exposed to a constant high temperature becomes visibly yellow over time. In this example, 3000 h was the furthest estimate, but the model can be used for longer estimates. The yellowing effect was visible on real test specimens photographed under D65 illumination.

3.2.2. *The prediction of appearance for a varying heat load*

Alternatively, we can predict the local colour change of a polymer product, if it is subjected to a known non-uniform heat load. This thermal load can be determined by measurement, analytical calculation or finite element simulation. For example, if heating pipes are placed over a sheet-like product (Fig. 8/a) and the heat load that the pipes will transfer to the product is known (e.g. a sinusoidally varying load Fig. 8/b), then the local colour change of the surface of the product can be determined (Fig. 8/c).

Once this has been determined, we can test our product against the quality requirements. For example, if the maximum permitted colour deviation ($\Delta E_{plate,\max}$) cannot be greater than 5, then we need to compare the least and most yellowed areas of the plate. The colour difference (ΔE_{plate}) can be estimated from the colour values of these areas according to Eq. (12):

$$\Delta E_{plate} = \sqrt{(L_{max} - L_{min})^2 + (a_{max} - a_{min})^2 + (b_{max} - b_{min})^2} \tag{12}$$

Fig. 8/d shows the colour difference of the sheet-like product as a function of time and TiO_2 content. If we want to reduce the colour change of the sheet with TiO_2, we can also obtain information on the amount of TiO_2-doping, so the minimum amount of TiO_2 to be used to meet the colour change specifications for the product can be determined based on the lifetime of the product (Fig. 8/f). In the present case, TiO_2

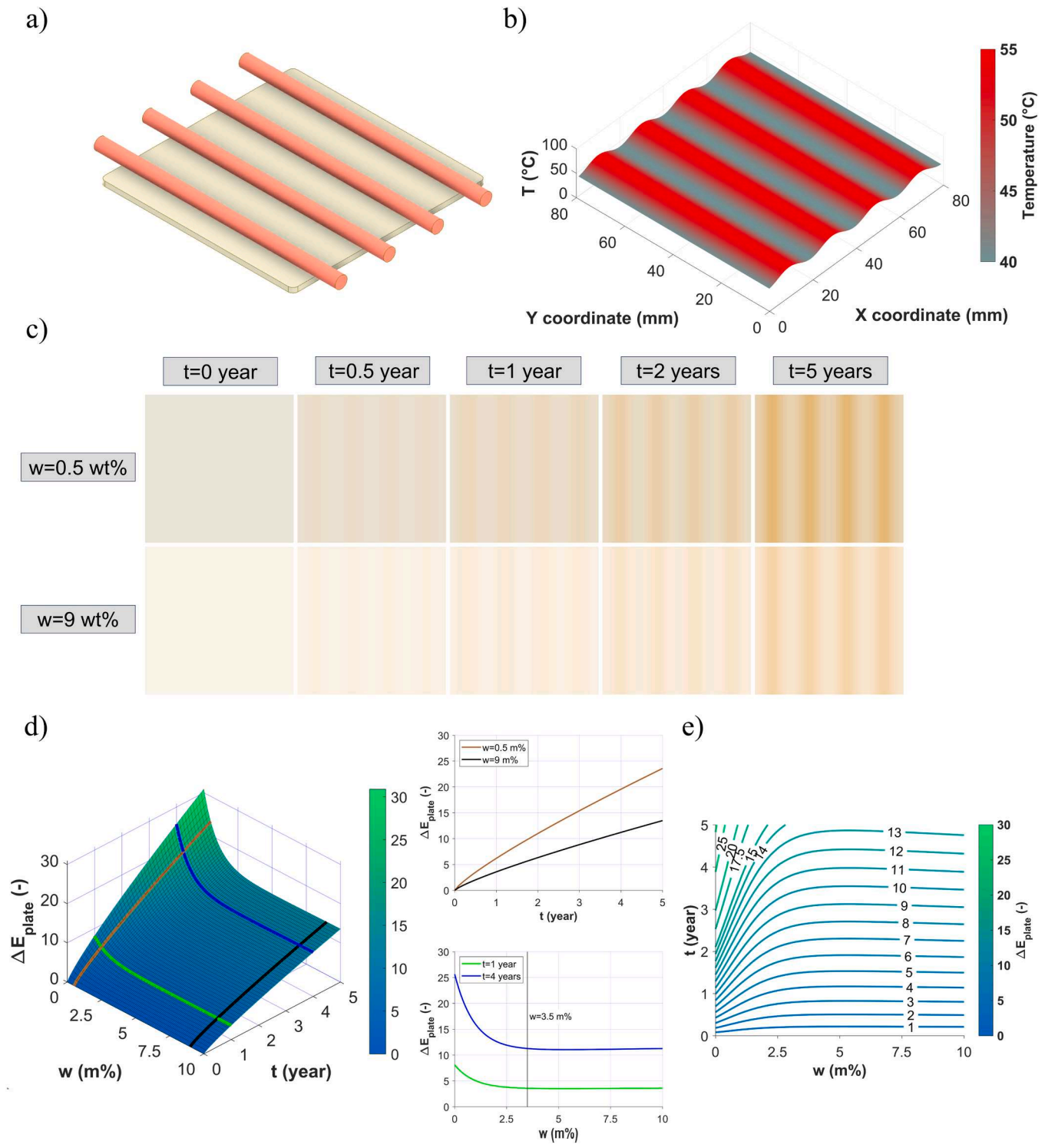

Fig. 8. Sheet-like product placed under heating pipes (a), heat load acting on the sheet-like product (b), surface colour predicted by the model for two different TiO_2 contents (c), surface plot for the colour difference of the sheet-like product (d) and nomogram to determine the optimal amount of TiO_2 (e).

doping higher than 3.5 wt% does not significantly improve temperature resistance. Using the methodology described above, nomograms can be generated to help determine the optimal amount of additives (Fig. 8/g). In engineering practice, such nomograms are very important as they simplify and accelerate the design process.

4. Conclusion

Our goal was to predict the thermal degradation–induced, long-term colour change of ABS-based TiO_2-doped products as a function of TiO_2 content and temperature. For this purpose, we investigated the colour change of ABS sheets doped with different levels of TiO_2 at five elevated temperatures between 60 and 100 °C. Applying the tTS principle and the CIELAB colour space, we proposed a methodology for developing a

robust model that can be used to estimate the long-term colour change of polymers doped with TiO_2, at elevated temperatures. We used 800 h of measurement data for model development and validated the colour change predictions of the model for up to 1600 h. At the application temperature range (below 80 °C), the average colour difference was <1.5 in all the examined cases, which is smaller than the just noticeable difference (JND) in the CIELAB colour space. To show the applicability of the model, we presented two simple case studies predicting the colour and appearance of a polymer product under constant and variable heat loads. The model's development and validation through 1600 h of CIELAB colour measurements under controlled thermal ageing provides a robust foundation for its use in simulation environments. This application enables manufacturers to forecast product appearance changes before production, supporting quality control and material optimisation for long-term aesthetics and stability.

Funding

This work was supported by the National Research, Development and Innovation Office, Hungary (OTKA FK138501). Ábris Dávid Virág is thankful for the support of the EKÖP-24–4-I-BME-201 University Research Fellowship Programme of the Ministry for Culture and Innovation from the source of the National Research, Development and Innovation Fund. Project no RRF-2.3.1–21–2022–00009, titled National Laboratory for Renewable Energy has been implemented with the support provided by the Recovery and Resilience Facility of the European Union within the framework of Programme Széchenyi Plan Plus. This research was funded by the Horizon Europe Framework Programme and the call HORIZON-WIDERA-2021-ACCESS-03, under the grant agreement for project 101,079,051 – IPPT_TWINN. Project no TKP-6–6/PALY-2021 has been implemented with the support provided by the Ministry of Culture and Innovation of Hungary from the National Research, Development and Innovation Fund, financed under the TKP2021-NVA funding scheme.

CRediT authorship contribution statement

Ábris Dávid Virág: Writing – original draft, Visualization, Validation, Software, Methodology, Investigation, Formal analysis, Conceptualization. **András Suplicz:** Writing – review & editing, Funding acquisition, Conceptualization. **Dániel Török:** Visualization, Validation, Software, Methodology, Investigation, Formal analysis, Conceptualization.

Declaration of competing interest

The authors declare that they have no known competing financial interests or personal relationships that could have appeared to influence the work reported in this paper.

Acknowledgements

We wish to thank ARBURG HUNGÁRIA KFT. for the ARBURG Allrounder injection moulding machine, and TOOL-TEMP HUNGÁRIA KFT., LENZKES GMBH and PIOVAN HUNGARY KFT. for the accessories.

Data availability

Data will be made available on request.

References

[1] J. Su, S. Wang, Influence of food packaging color and foods type on consumer purchase intention: the mediating role of perceived fluency, Front. Nutr. 10 (2023), https://doi.org/10.3389/fnut.2023.1344237.
[2] K. Steiner, A. Florack, The influence of packaging color on consumer perceptions of healthfulness: a systematic review and theoretical framework, Foods (2023) 12, https://doi.org/10.3390/foods12213911.
[3] C. Spence, On the psychological impact of food colour, Flavour 4 (2015) 21, https://doi.org/10.1186/s13411-015-0031-3.
[4] H. Hagtvedt, S.A. Brasel, Color Saturation Increases Perceived Product Size, J. Consum. Res. 44 (2017) 396–413, https://doi.org/10.1093/jcr/ucx039.
[5] F. Salehi, K. Goharpour, H. Razavi Kamran, Effects of different pretreatment techniques on the color indexes, drying characteristics and rehydration ratio of eggplant slices, Result. Eng. 21 (2024) 101690, https://doi.org/10.1016/J.RINENG.2023.101690.
[6] R. Cheng, Y. Guo, Study on the effect of heat treatment on amethyst color and the cause of coloration, Sci. Rep. 10 (2020) 14927, https://doi.org/10.1038/s41598-020-71786-1.
[7] A.Z. Abidin, S. Steven, R. Fadli, M.F. Nabiel, E.V. Yemensia, E.S.A. Soekotjo, A. A. Rahman Setiawan, N.A. Sasongko, H.P. Rendra Graha, T. Abidin, R.P. Putra, Influence of several physical parameters in enzymatic fermentation of vegetable and fruit waste to produce organic liquid fertilizer using MASARO technology, Result. Eng. 23 (2024) 102567, https://doi.org/10.1016/J.RINENG.2024.102567.
[8] P. Torniainen, D. Jones, D. Sandberg, Colour as a quality indicator for industrially manufactured ThermoWood®, Wood Mater. Sci. Eng. 16 (2021) 287–289, https://doi.org/10.1080/17480272.2021.1958920.
[9] C. Victor Ossia, K. Hosung, L.V. Markova, Utilization of color change in the condition monitoring of synthetic hydraulic oils, Ind. Lubr Tribol. 62 (2010) 349–355, https://doi.org/10.1108/00368791011076245.
[10] Y. Meng, Y. Cao, H. Ji, J. Chen, Z. He, Z. Long, C. Dong, Fabrication of environmental humidity-responsive iridescent films with cellulose nanocrystal/polyols, Carbohydr. Polym. 240 (2020) 116281, https://doi.org/10.1016/J.CARBPOL.2020.116281.
[11] M. Momtaz, J. Chen, High-Performance Colorimetric Humidity Sensors Based on Konjac Glucomannan, ACS Appl. Mater. Interfaces 12 (2020) 54104–54116, https://doi.org/10.1021/acsami.0c16495.
[12] G. Gao, Q. Li, H. Luo, X. Huang, Preparation and performance evaluation of humidity-sensitive color-changing materials via hyperspectral imaging, Sens. Actuators A Phys. 362 (2023) 114660, https://doi.org/10.1016/J.SNA.2023.114660.
[13] L. Yang, J. Meng, L. Yu, X. Gao, Y. Chen, Y. Wang, T. Xue, Y. Liu, C. Zhi, Reversible dual-responsive color-changing fabric based on thermochromic microcapsules for textile fashion and intelligent monitoring, Dyes. Pigm. 231 (2024) 112397, https://doi.org/10.1016/J.DYEPIG.2024.112397.
[14] A. Lerma-Canto, I. Dominguez-Candela, J. Gomez-Caturla, V. Fombuena, D. Garcia-Garcia, Efficient single-step reactive compatibilization of hemp flour-reinforced PLA/TPS blends: exploring eco-friendly alternatives and bio-based compatibilizers from maleinized hemp oil, Express Polym. Lett. 18 (2024) 214–228, https://doi.org/10.3144/expresspolymlett.2024.15.
[15] J.T. Guthrie, Polymeric colorants, review of progress in coloration and related topics 20 (1990) 40–52. https://doi.org/10.1111/j.1478-4408.1990.tb00073.x.
[16] R. Mia, M.A. Bakar, M.R. Islam, T. Ahmed, Eco-friendly coloration from mahogany wood waste for sustainable dyeing of organic nonwoven cotton fabric, Result. Eng. 17 (2023) 101032, https://doi.org/10.1016/J.RINENG.2023.101032.
[17] M. Edge, R. Wiles, N.S. Allen, W.A. McDonald, S.V. Mortlock, Characterisation of the species responsible for yellowing in melt degraded aromatic polyesters—I: yellowing of poly(ethylene terephthalate), Polym. Degrad. Stab. 53 (1996) 141–151, https://doi.org/10.1016/0141-3910(96)00081-X.
[18] N.S. Allen, M. Edge, S. Hussain, Perspectives on yellowing in the degradation of polymer materials: inter-relationship of structure, mechanisms and modes of stabilisation, Polym. Degrad. Stab. 201 (2022) 109977, https://doi.org/10.1016/j.polymdegradstab.2022.109977.
[19] G. Pastorelli, C. Cucci, O. Garcia, G. Piantanida, A. Elnaggar, M. Cassar, M. Strlič, Environmentally induced colour change during natural degradation of selected polymers, Polym. Degrad. Stab. 107 (2014) 198–209, https://doi.org/10.1016/j.polymdegradstab.2013.11.007.
[20] C. Wu, B.C. Meng, L. Tam, L. He, Yellowing mechanisms of epoxy and vinyl ester resins under thermal, UV and natural aging conditions and protection methods, Polym. Test. 114 (2022) 107708, https://doi.org/10.1016/j.polymertesting.2022.107708.
[21] T. Achtioui, C. Lacoste, M.Le Baillif, D. Erre, Prediction of the yellowing of styrene-stat-acrylonitrile and acrylonitrile-butadiene-styrene during processing in an internal mixer, 38 (2018) 983–993. https://doi.org/10.1515/polyeng-2017-0305.
[22] M. Matsuo, M. Yokoyama, K. Umemura, J. Gril, K. Yano, S. Kawai, Color changes in wood during heating: kinetic analysis by applying a time-temperature superposition method, Appl. Phys. A 99 (2010) 47–52, https://doi.org/10.1007/s00339-010-5542-2.
[23] K. Mochizuki, K. Takayama, Prediction of color changes using the time–temperature superposition principle in liquid formulations, Chem. Pharm. Bull. (Tokyo) 62 (2014) 1225–1230, https://doi.org/10.1248/cpb.c14-00530.
[24] D. Wu, D. Zhang, S. Liu, Z. Jin, T. Chowwanonthapunya, J. Gao, X. Li, Prediction of polycarbonate degradation in natural atmospheric environment of China based on BP-ANN model with screened environmental factors, Chem. Eng. J. 399 (2020) 125878, https://doi.org/10.1016/j.cej.2020.125878.
[25] F. Liu, L. Jiang, S. Yang, Ultra-violet degradation behavior of polymeric backsheets for photovoltaic modules, Sol. Energy 108 (2014) 88–100, https://doi.org/10.1016/j.solener.2014.06.027.
[26] N.S. Allen, M. Edge, A. Ortega, G. Sandoval, C.M. Liauw, J. Verran, J. Stratton, R. B. McIntyre, Degradation and stabilisation of polymers and coatings: nano versus

pigmentary titania particles, Polym. Degrad. Stab. 85 (2004) 927–946, https://doi.org/10.1016/j.polymdegradstab.2003.09.024.
[27] U. Gesenhues, Influence of titanium dioxide pigments on the photodegradation of poly(vinyl chloride), Polym. Degrad. Stab. 68 (2000) 185–196, https://doi.org/10.1016/S0141-3910(99)00184-6.
[28] J.J. Perez Bravo, M.E. Villanueva, G.I. Tovar, N.J. François, G.J. Copello, Visible-light enhanced photocatalytic performance by lowering the bandgap of reusable TiO2/chitin and ZnO/chitin nanocomposites for trimethoprim degradation, Express Polym. Lett. 16 (2022) 1177–1192, https://doi.org/10.3144/expresspolymlett.2022.86.
[29] R.E. Day, The role of titanium dioxide pigments in the degradation and stabilisation of polymers in the plastics industry, Polym. Degrad. Stab. 29 (1990) 73–92, https://doi.org/10.1016/0141-3910(90)90023-Z.
[30] O.V. Semperger, Z. Osváth, S. Pásztor, A. Suplicz, The effect of the titanium dioxide nanoparticles on the morphology and degradation of polyamide 6 prepared by anionic ring-opening polymerization, Polym. Eng. Sci. 62 (2022) 2079–2088, https://doi.org/10.1002/pen.25990.
[31] S. Asiaban, S.F. Taghinejad, Investigation of the effect of titanium dioxide on optical aspects and physical and mechanical characteristics of ABS polymer, J. Elastomers Plast. 42 (2010) 267–274, https://doi.org/10.1177/0095244310368128.
[32] L. Han, L. Shen, H. Lin, Z. Huang, Y. Xu, R. Li, B. Li, C. Chen, W. Yu, J. Teng, 3D printing titanium dioxide-acrylonitrile-butadiene-styrene (TiO2-ABS) composite membrane for efficient oil/water separation, Chemosphere 315 (2023) 137791, https://doi.org/10.1016/j.chemosphere.2023.137791.
[33] J.D. Ferry, Viscoelastic Properties of Polymers, 3rd ed., John Wiley&Sons, New York, 1980.
[34] Y. Chen, R. Liu, J. Luo, Enhancing weathering resistance of UV-curable coatings by using TiO2 particles as filler, Prog. Org. Coat. 169 (2022) 106936, https://doi.org/10.1016/J.PORGCOAT.2022.106936.
[35] T.V. Nguyen, P.H. Dao, T.A. Nguyen, V.P. Mac, T.V. Do, T.M.L. Dang, M.N. Ha, H. N. Trinh, T.L. Le, D.L. Tran, T.D. Nguyen, P. Nguyen-Tri, Effects of nano-TiO2 and nano-SiO2 particles on the reflectance and weathering durability of solar heat reflectance coating, J. Photochem. Photobiol. A Chem. 442 (2023) 114752, https://doi.org/10.1016/J.JPHOTOCHEM.2023.114752.
[36] J.D. Bersch, A.B. Masuero, D.C.C. Dal Molin, Photocatalytic coloured rendering mortars: effect of TiO2 and iron oxide pigments on the physical, mechanical, hygric, and photoactive behaviour, Mater. Struct. 56 (2023) 146, https://doi.org/10.1617/s11527-023-02240-7.
[37] M.I. Mohammed, D. Wilson, E. Gomez-Kervin, B. Tang, J. Wang, Investigation of closed-loop manufacturing with acrylonitrile butadiene styrene over multiple generations using additive manufacturing, ACS Sustain. Chem. Eng. 7 (2019) 13955–13969, https://doi.org/10.1021/acssuschemeng.9b02368.
[38] G. Sharma, Color fundamentals for digital imaging, in: G. Sharma (Ed.), Digital Color Imaging Handbook,, 1st edition, CRC Press, New York, 2003.